On the Joint Impact of UAV Orientation Instability and Phase Errors in UAV-Aided RIS Systems

Sourosmita Das, Manojkumar B. Kokare, Prashant Sharma, Swaminathan R., Sumit Gautam, and Saptarshi Ghosh
Department of Electrical Engineering, Indian Institute of Technology Indore, India
Emails: mt2402102010@iiti.ac.in, phd2201102016@iiti.ac.in, phd2301102004@iiti.ac.in
swamiramabadran@iiti.ac.in, sumit.gautam@iiti.ac.in, sghosh@iiti.ac.in

***Abstract*—Uncrewed aerial vehicle (UAV)-mounted reconfigurable intelligent surface (RIS) platforms offer a flexible solution for extending wireless coverage in obstructed, disaster-affected, and infrastructure-constrained environments. However, practical UAV platforms experience orientation fluctuations and RIS phase estimation errors that can significantly degrade communication performance, yet their joint impact remains insufficiently explored. This paper analyzes the performance of UAV-assisted RIS communication systems under Nakagami-m fading while accounting for stochastic UAV angular deviations and RIS phase errors. The phase errors are modeled using the von Mises distribution, and the RIS radiation pattern under UAV orientation fluctuations is characterized through linear approximation and sector-based modeling to obtain its statistical representation. Based on this framework, analytical expressions for the outage probability (OP), average symbol error rate (ASER), and ergodic capacity (EC) are derived. Monte-Carlo simulations validate the analytical results and demonstrate the notable performance degradation caused by the combined effects of angular fluctuations and phase uncertainties, offering valuable insights for the reliable design of UAV-mounted RIS (URIS)-assisted communication systems.**

***Index Terms*—Nakagami-m fading, orientation deviations, phase estimation errors, reconfigurable intelligent surfaces (RIS), UAV-mounted RIS (URIS) and uncrewed aerial vehicles (UAV).**

I. Introduction

Reconfigurable intelligent surfaces (RIS) have recently garnered considerable attention due to their ability to manipulate the wireless propagation environment through programmable signal reflection with low hardware complexity and energy consumption. RIS can improve signal coverage, reliability, and energy efficiency (EE) of a wireless environment by adjusting the phase shifts of reflecting elements [1]. In parallel, uncrewed aerial vehicles (UAVs) are being actively explored as flexible aerial platforms capable of rapidly establishing wireless connectivity in environments where conventional infrastructure is unavailable or damaged. [2]. The integration of RIS with UAV platforms combines aerial mobility with adaptive propagation control, enabling dynamic three-dimensional (3D) positioning and virtual line-of-sight (LoS) links between transmitters and obstructed receivers [3]. Such UAV-aided RIS systems offer a promising solution for emergency response, disaster recovery, and coverage extension in infrastructure-limited or dense urban scenarios. Motivated by the potential of RIS-aided communications, several studies have investigated their performance under various channel conditions. In [4], the authors analyzed multi-RIS-assisted networks under Nakagami-m fading and derived closed-form approximations for outage probability (OP) and average symbol error probability (SEP) to characterize system reliability. Similarly, cooperative communication systems assisted by multiple RISs were studied in [5], where performance improvements from combining direct and reflected links were evaluated via SEP analysis. More recently, the integration of RIS with UAVs has attracted significant interest due to the flexibility of aerial deployment and dynamic positioning. In [6], a theoretical framework for UAV-borne reflecting surfaces was proposed to analyze OP, ergodic capacity (EC), and EE.

In practical deployments, RIS performance is affected by phase estimation errors, hardware imperfections, and UAV hovering fluctuations. For instance, the impact of phase shift errors modeled using a Von Mises distribution on outage performance was investigated in [7], while [8] analyzed UAV-mounted RIS systems by characterizing the 3D radiation pattern and deriving closed-form outage probability expressions. Despite these advancements, most existing studies consider these impairments independently and assume ideal conditions such as stable UAV platforms and accurate RIS phase control. In practice, UAV-mounted RIS systems may experience stochastic orientation deviations during hovering, while RIS phase adjustments may suffer from estimation errors. Since UAV orientation fluctuations affect the effective radiation gain and RIS phase errors degrade coherent signal combining, their joint presence can lead to coupled performance degradation that cannot be accurately captured through separate analyses. The combined impact of these impairments on system performance remains largely unexplored.

Motivated by this gap, this paper investigates the joint impact of stochastic UAV orientation deviations and phase estimation errors on the performance of UAV-aided RIS communication systems under Nakagami-m fading channels. The primary contributions of this work are summarized as follows:

- We have developed an analytical framework for UAV-aided RIS communication systems over Nakagami-m fading channels, accounting for practical system impairments.
- The impact of stochastic UAV orientation deviations during hovering on the RIS radiation pattern is characterized using linear approximation and sector-based modeling of

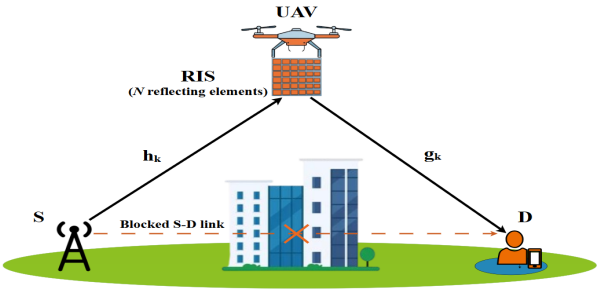

Fig. 1: System model of UAV-aided RIS communication system.

the 3D radiation pattern.

- RIS phase estimation errors are incorporated and modelled using the von Mises distribution to capture practical phase imperfections.
- The closed-form expressions for OP and tractable approximate expressions for ASER and EC based on Gauss–Laguerre (GL) quadrature are derived by accounting for the joint impact of UAV angular fluctuations and RIS phase errors.
- Monte-Carlo simulations validate the analytical results and provide insights into the performance degradation caused by these practical impairments.

II. System and Channel Models

We have considered a UAV-aided RIS communication system, where a UAV-mounted RIS (URIS) enables communication between a source S and a destination D in the absence of a direct link due to severe blockage, as shown in Fig. 1. The URIS facilitates transmission by reflecting the signal from S toward D through the appropriate phase configuration of its N reflecting elements. The locations of S and D are represented in Cartesian coordinates as $\mathbf{v}_s = (x_s, y_s, 0)$ and $\mathbf{v}_d = (x_d, y_d, 0)$, respectively, since both nodes are positioned on the ground. The URIS is deployed at altitude h with coordinates $\mathbf{v}_u = (x_u, y_u, h)$. The horizontal projections of these nodes on the two-dimensional plane are denoted by $\mathbf{w}_s = (x_s, y_s)$, $\mathbf{w}_d = (x_d, y_d)$, and $\mathbf{w}_u = (x_u, y_u)$. Accordingly, the elevation angles corresponding to the S-to-URIS and URIS-to-D links are given by $\theta_u = \arctan\left(\frac{h}{|\mathbf{w}_u - \mathbf{w}_s|}\right)$ and $\theta_d = \arctan\left(\frac{h}{|\mathbf{w}_u - \mathbf{w}_d|}\right)$, respectively [9].

The elevation angles play a crucial role in determining the propagation characteristics. In particular, the probability of establishing a LoS connection depends on the elevation angle between the URIS and the communicating node. Accordingly, the LoS probability for link i, where $i \in \{u, d\}$, is modeled as

$$p_L(\theta_i) = \left(1 + l_i \exp(-n_i(\theta_i - l_i))\right)^{-1}, \tag{1}$$

where l_i and n_i are environment-dependent parameters obtained from empirical measurements for air-to-ground propagation environments [9]. Furthermore, the path-loss exponent is also influenced by the elevation angle and is modeled as

$$\alpha(\theta_i) = p_L(\theta_i) k_i + w_i, \tag{2}$$

where k_i and w_i are constants associated with the uplink and downlink channels [10].

The small-scale fading for the S–to-URIS and URIS–to-D links is modeled using the Nakagami-m fading distribution due to its flexibility in characterizing different propagation conditions. Accordingly, the signal received at D through the N URIS elements can be expressed as [6]

$$y_i = \sum_{k=1}^{N} \sqrt{A p_u d_u^{-\alpha(\theta_u)}} \bar{h}_k e^{j\phi_k} \sqrt{A d_d^{-\alpha(\theta_d)}} \bar{g}_k x + w_u, \tag{3}$$

where $\bar{h}_k = h_k e^{j\phi_u}$ denotes the channel coefficient between S and the k^{th} URIS element and $\bar{g}_k = g_k e^{j\phi_d}$ represents the channel coefficient between the k^{th} URIS[1] element and D. The magnitude of the channel coefficients h_k and g_k follow independent Nakagami-m distributions with parameters $(m_{k,1}, \Omega_{k,1})$ and $(m_{k,2}, \Omega_{k,2})$, respectively. Here, ϕ_u and ϕ_d denote the phases associated with the respective channels, while ϕ_k represents the phase shift due to the k^{th} URIS element. In (3), x denotes the transmitted signal, p_u is the transmit power at S, and w_u represents additive white Gaussian noise (AWGN) with variance N_0. The parameter A captures system-dependent constants such as antenna gains and carrier frequency effects, whereas d_u and d_d denote the distances of the S-to-URIS and URIS-to-D links, respectively.

Let $z_k = h_k g_k$ denote the cascaded channel gain corresponding to the k^{th} URIS element. By utilizing the distribution of the product of two independent random variables, the probability density function (PDF) of z_k is expressed as [4]

$$f_{z_k}(x) = \frac{4(\Theta_{k,1}\Theta_{k,2})^{m_{k,1}+m_{k,2}}}{\Gamma(m_{k,1})\Gamma(m_{k,2})} K_{m_{k,1}-m_{k,2}}\left(2\Theta_{k,1}\Theta_{k,2}x\right) \times x^{m_{k,1}+m_{k,2}-1}, \tag{4}$$

where $\Theta_{k,j} = \sqrt{\frac{m_{k,j}}{\Omega_{k,j}}}$ for $j \in \{1, 2\}$, $\Gamma(\cdot)$ denotes the Gamma function, and $K_\nu(\cdot)$ represents the modified Bessel function of the second kind with order ν. Now, the r^{th} moment of z_k is obtained using (4) as [4]

$$\mathbb{E}[z_k^r] = \frac{\Gamma\left(m_{k,1} + \frac{r}{2}\right)\Gamma\left(m_{k,2} + \frac{r}{2}\right)}{(\Theta_{k,1}\Theta_{k,2})^r \Gamma(m_{k,1})\Gamma(m_{k,2})}. \tag{5}$$

In practical UAV-mounted RIS systems, maintaining a perfectly stable orientation during hovering is challenging due to environmental disturbances such as wind and mechanical vibrations. These effects introduce random orientation deviations, which in turn disturb the alignment between the URIS and the communicating nodes, thereby impacting the reflected signal power. The UAV angular deviations are modeled as $\epsilon_x \sim \mathcal{N}(0, \sigma_x^2)$ and $\epsilon_y \sim \mathcal{N}(0, \sigma_y^2)$ corresponding to the deviations in the x–z and y–z planes, respectively [8], which introduce fluctuations in the effective RIS radiation pattern. To capture this effect, an effective radiation gain G is introduced [8], which accounts for variations in the received signal strength due to UAV orientation fluctuations. The normalized radiation gain is expressed as $G = G_e \times G_a$, where G_e

[1]Under perfect phase adjustment, the RIS controller compensates the phases of the cascaded channel by selecting $\phi_k = -(\phi_u + \phi_d)$, which ensures coherent signal combining at the destination.

denotes the radiation pattern of an individual RIS element and G_a represents the array factor. Owing to random angular deviations, the radiation gain G becomes an RV[2]. Using the sector-based approximation, its distribution is modeled as

$$f_G(G) = \sum_{i=1}^{J} p(i)\delta(G - q(i)), \tag{6}$$

where J depends on the number of sectors, and $q(i)$ and $p(i)$ denote the discrete radiation gain levels and their corresponding probabilities, respectively.

In addition, practical RIS implementations may suffer from phase estimation errors due to hardware imperfections and the finite resolution of phase shifters. Accordingly, the phase shift at the k^{th} RIS element is modeled as $\phi_k = \phi_k^{\text{opt}} + \theta_{\text{err}}$, where ϕ_k^{opt} is the optimal phase for coherent signal combining and θ_{err} represents the phase estimation error. The phase error θ_{err} follows a von Mises distribution[3], and its PDF is given as [7]

$$f_{\theta_{err}}(x) = \frac{e^{\kappa \cos(x)}}{2\pi I_0(\kappa)}, \tag{7}$$

where κ is the concentration parameter and $I_0(\cdot)$ denotes the modified Bessel function of the first kind of order zero. The trigonometric moments are given by $\phi_p = \mathbb{E}[e^{jp\theta_{err}}] = \frac{I_p(\kappa)}{I_0(\kappa)}$. Including the URIS phase errors, the cascaded channel gain due to N URIS elements can be written as $v = \sum_{k=1}^{N} z_k e^{j\theta_{err}}$, where v represents the sum of independent phase-impaired channel contributions. Its distribution can be accurately approximated using the first term of a Laguerre series expansion, resulting in a Gamma distribution with PDF given by

$$f_v(x) \approx \frac{1}{\Gamma(a_k) b_k^{a_k}} x^{a_k - 1} \exp\left(-\frac{x}{b_k}\right), \tag{8}$$

where $a_k = \frac{(\mathbb{E}[v])^2}{\text{Var}(v)}$ and $b_k = \frac{\text{Var}(v)}{\mathbb{E}[v]}$. Using the statistical properties of Nakagami-m fading and the trigonometric moments of the von Mises distributed phase error, the mean and variance of the channel gain v can be expressed as $\mathbb{E}[v] = N\mu_1\phi_1$ and $\text{Var}(v) = N\sigma^2\left(\frac{1+\phi_2}{2}\right) + N\mu_1^2\left(\frac{1+\phi_2}{2} - \phi_1^2\right)$, respectively, where μ_1 and μ_2 denote the first and second moments of z_k and $\sigma^2 = \mu_2 - \mu_1^2$. The corresponding CDF of v can be obtained by integrating the PDF in (8), as

$$F_v(v) = \frac{\gamma(a_k, \frac{v}{b_k})}{\Gamma(a_k)}, \tag{9}$$

where $\gamma(\cdot,\cdot)$ denotes the lower incomplete Gamma function and $\Gamma(\cdot)$ represents the complete Gamma function.

The instantaneous SNR of the proposed system, accounting for UAV orientation deviations and phase errors, is given by

$$\gamma = \gamma_0 G U, \tag{10}$$

where $\gamma_0 = \frac{A^2 p_u}{N_0} d_u^{-\alpha(\theta_u)} d_d^{-\alpha(\theta_d)}$ and $U = |v|^2$.

[2]When UAV orientation fluctuations are neglected, the radiation gain becomes deterministic with $G = 1$, reducing the model to the conventional RIS-assisted system.

[3]In the absence of phase errors (i.e., $\theta_{\text{err}} = 0$), the cascaded channel reduces to $v = \sum_{k=1}^{N} z_k$, corresponding to perfect phase alignment.

Using the instantaneous SNR expression in (10), the PDF in (8), conditioned on the radiation gain G, is obtained via transformation of RVs as

$$f_{\gamma|G}(\gamma|G) = \frac{1}{2\Gamma(a_k) b_k^{a_k}} (\gamma_0 G)^{-\frac{a_k}{2}} \gamma^{\frac{a_k}{2}-1} \exp\left(-\frac{\sqrt{\frac{\gamma}{\gamma_0 G}}}{b_k}\right). \tag{11}$$

Accordingly, the conditional CDF of the instantaneous SNR can be expressed as

$$F_{\gamma|G}(\gamma|G) = F_v\left(\sqrt{\frac{\gamma}{\gamma_0 G}}\right) = \frac{\gamma\left(a_k, \frac{\sqrt{\gamma/(\gamma_0 G)}}{b_k}\right)}{\Gamma(a_k)}. \tag{12}$$

Since the radiation gain G is a RV, the unconditional CDF of the instantaneous SNR is obtained by averaging the conditional CDF over the distribution of G as

$$F_\gamma(\gamma) = \mathbb{E}_G\left[F_{\gamma|G}(\gamma|G)\right] \tag{13}$$

Using (6) and (12), the above CDF expression for instantaneous SNR is written as

$$F_\gamma(\gamma) = \sum_{i=1}^{J} p(i)\, F_v\left(\sqrt{\frac{\gamma}{\gamma_0 q(i)}}\right), \tag{14}$$

where $F_v(\cdot)$ is given by (9).

III. Performance Analysis

1) Outage Probability: OP is the probability that the instantaneous received SNR falls below a predefined threshold value γ_{th}. So, the OP is expressed as $F_\gamma(\gamma_{th})$, where $F_\gamma(\cdot)$ is given by (14).

2) Average Symbol Error Rate: The ASER of the proposed system under M-ary phase shift keying (M-PSK) modulation can be derived using the CDF as [11]

$$P_{ser} = \frac{p\sqrt{q}}{2\sqrt{2\pi}} \int_0^\infty F_\gamma(\gamma)\gamma^{-1/2} e^{-\frac{q\gamma}{2}} d\gamma, \tag{15}$$

where $q = sin(\frac{\pi}{M})$, modulation order $M = 2^n$, $p = 0.5$ for binary phase shift keying (BPSK) and $p = 1$ for $n \geq 2$ [11]. Due to mathematical complexity, we have used the n-point GL quadrature method to solve (15). Accordingly, the ASER can be approximated as

$$P_{ser} \approx \frac{p\sqrt{q}}{2\sqrt{2\pi}} \sum_{i=1}^{J} p(i) \sum_{l=1}^{n} W_l F_v\left(\sqrt{\frac{\phi_l}{\gamma_0 q(i)}}\right), \tag{16}$$

where $F_v(\cdot)$ is given by (9), W_l and ϕ_l denote the GL quadrature weights and roots, respectively [11].

3) Ergodic Capacity: The normalized channel capacity (in bit/s/Hz) characterizes the maximum achievable data rate under reliable communication conditions. The EC of the proposed system is evaluated using the CDF of the equivalent channel as [11]

$$C = \frac{1}{\ln 2} \int_0^\infty \frac{1 - F_\gamma(\gamma)}{1 + \gamma}\, d\gamma \tag{17}$$

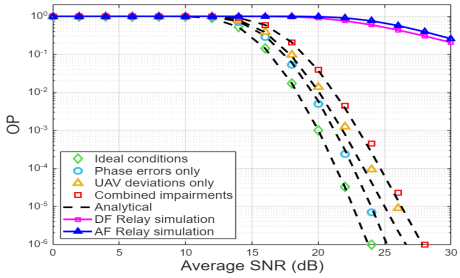

Fig. 2: OP versus average SNR for URIS-assisted (ideal/impaired) and AF/DF relaying systems.

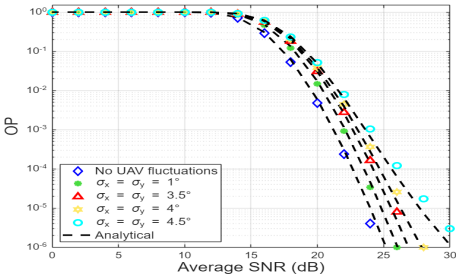

Fig. 3: OP versus average SNR for varying UAV fluctuation severity.

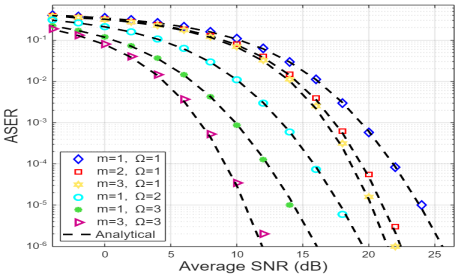

Fig. 4: ASER versus average SNR for varying m and Ω values.

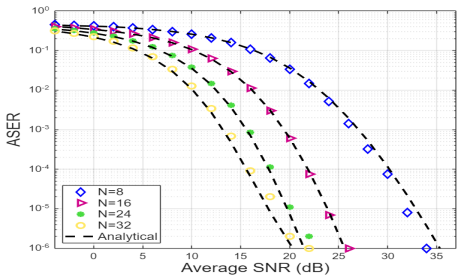

Fig. 5: ASER versus average SNR for varying N values.

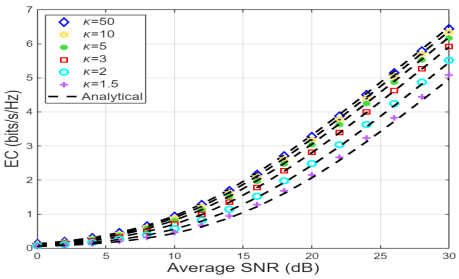

Fig. 6: EC versus average SNR for varying phase error severity.

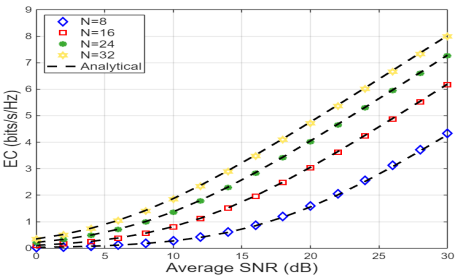

Fig. 7: EC versus average SNR for varying N values.

Now, due to mathematical complexity, we utilize the GL quadrature method to calculate the EC. After applying the GL approximation, (17) is written as

$$C \approx \frac{1}{\ln 2} \sum_{i=1}^{J} p(i) \sum_{l=1}^{n} W_l e^{\phi_l} \frac{1 - F_v\left(\sqrt{\frac{\phi_l}{\gamma_0 q(i)}}\right)}{1 + \phi_l}. \tag{18}$$

IV. Results and Discussion

In this section, numerical results are presented to evaluate the performance of the UAV-assisted RIS communication system under practical impairments. The derived analytical expressions are validated via Monte-Carlo simulations with 10^6 realizations, demonstrating excellent agreement with the theoretical results. Unless otherwise specified, identical Nakagami-m fading parameters are assumed for the S-to-URIS and URIS-to-D links, i.e., $m_{k,1} = m_{k,2} = m = 1$ and $\Omega_{k,1} = \Omega_{k,2} = \Omega = 1$. The outage threshold is set to $\gamma_{\text{th}} = 5$ dB, and the number of RIS elements is fixed at $N = 16$. For ASER analysis, BPSK modulation is considered. Practical impairments are incorporated by modeling RIS phase errors using a von Mises distribution with a concentration parameter $\kappa = 5$, while UAV orientation fluctuations follow Gaussian angular deviations with $\sigma_x = \sigma_y = 4°$. Furthermore, the close agreement between analytical and simulation curves demonstrates that the derived closed-form OP and the GL-based approximate expressions for ASER and EC are highly accurate.

In Fig. 2, the OP versus average SNR is presented for both ideal and impaired conditions, including RIS phase errors, UAV orientation deviations, and their combined effect, and is compared with conventional AF and DF relaying schemes. As expected, ideal conditions yield the best performance, while impairments degrade OP, with the combined case exhibiting the worst performance. Specifically, at an SNR of 20 dB, the ideal case, phase-error-only case, UAV-orientation-deviation-only case, and combined impairment scenarios achieve OP values of 10^{-3}, 5×10^{-3}, 10^{-2}, and 4×10^{-2}, respectively. This indicates performance degradation with increasing impairments, mainly due to phase misalignment and beam misdirection, which reduce beamforming gain and received signal power. Furthermore, the proposed RIS-assisted framework outperforms conventional AF and DF relaying due to coherent beamforming gain, while DF achieves better performance than AF by mitigating noise propagation through decoding.

In Fig. 3, the OP performance is evaluated for different values of UAV angular deviations, i.e., $\sigma_x = \sigma_y = \sigma$. It is observed that increasing σ leads to a progressive degradation in OP performance. In the absence of jitter ($\sigma = 0$), corresponding to a perfectly stable UAV, the system achieves the best performance due to accurate beam alignment and maximum array gain. As σ increases, random orientation fluctuations distort the effective radiation pattern of the UAV-mounted RIS, resulting in beam misalignment and reduced received signal power. At an average SNR of 25 dB, the OP values for $\sigma = 0°$, $1°$, $3.5°$, $4°$, and $4.5°$ are 1.4×10^{-6}, 7×10^{-6}, 2.5×10^{-5}, 6×10^{-5}, and 2×10^{-4}, respectively. This degradation is attributed to hovering-induced instability, which limits the effectiveness of coherent signal combining.

In Fig. 4, the ASER performance is evaluated for different values of the Nakagami-m fading parameters m and Ω. It is observed that increasing m improves the ASER performance, as larger values of m correspond to less severe fading and more reliable channel conditions. Notably, the case $m = 1$

reduces to the Rayleigh fading scenario. Similarly, increasing Ω enhances average received power, resulting in a leftward shift of the ASER curves, i.e., improved performance at lower SNR values. For a target ASER of 10^{-4}, the configuration $(m, \Omega) = (3, 3)$ achieves SNR gains of 3.5 dB, 7 dB, 9.5 dB, 10.5 dB, and 13 dB compared to $(1, 3)$, $(1, 2)$, $(3, 1)$, $(2, 1)$, and $(1, 1)$, respectively. Varying Ω from 1 to 3 (with fixed $m = 1$) provides a more pronounced performance improvement compared to varying m from 1 to 3 (with fixed $\Omega = 1$). This behavior can be explained by the distinct roles of the two parameters. Specifically, increasing m reduces the severity of fading by mitigating channel fluctuations; however, it does not directly enhance the average received signal power. In contrast, increasing Ω directly scales the average channel gain, resulting in a higher effective SNR. Consequently, improvements in Ω lead to a more significant enhancement in ASER performance compared to increasing m, particularly in moderate-to-high SNR regimes where signal power dominates over fading effects.

Fig. 5 shows the impact of the number of reflecting elements N on ASER performance. Increasing N from 8 to 32 significantly improves performance due to enhanced array gain and more effective coherent signal combining. To achieve an ASER of 10^{-3}, the configuration with $N = 32$ provides SNR gains of approximately 2.5 dB, 6.5 dB, and 14 dB compared to $N = 24$, $N = 16$, and $N = 8$, respectively. Moreover, increasing N from 8 to 24 yields an approximate 98.8% improvement in ASER at an SNR of 15 dB. This enhancement is due to the increased beamforming gain achieved by constructively combining the reflected signals, which boosts the received signal power. A larger number of RIS elements provides improved spatial diversity and an averaging effect over multiple propagation paths, thereby reducing channel fluctuations and mitigating deep fades.

In Fig. 6, the EC performance is evaluated for different values of the phase error concentration parameter κ. It is observed that increasing κ improves the EC performance, since larger κ corresponds to reduced phase uncertainty and improved phase alignment. At an SNR of 25 dB, the EC values for $\kappa = 1.5, 2, 3, 5, 10$, and 50 are 3.4, 3.9, 4.3, 4.6, 4.75, and 4.9 bit/s/Hz, respectively. EC increases rapidly as κ grows from 1.5 to 10; however, beyond $\kappa = 10$, the performance improvement becomes marginal, and the EC tends to saturate. For small κ, widely spread phase errors cause significant misalignment and reduced coherent combining. As κ increases, the errors concentrate around the optimal phase, improving constructive combining and effective SNR. However, for large κ, phase errors become negligible and the system approaches ideal conditions, resulting in performance saturation with minimal additional gain.

In Fig. 7, the EC is evaluated for different values of the number of RIS elements N. Increasing N significantly enhances the EC due to the improved passive beamforming gain. At an SNR of 25 dB, as N increases from 8 to 32, the system capacity improves by approximately 129%. This improvement arises because the reflected signal power scales with N, resulting in higher effective channel gain and SNR. Furthermore, the capacity requirements of enhanced mobile broadband (eMBB) scenarios can be satisfied at SNR ≤ 25 dB for $N \geq 32$. In contrast, for smaller values of N, higher transmit power is required to achieve the same capacity. This highlights the trade-off between the number of RIS elements and transmit power, where increasing N can effectively reduce the required SNR, while maintaining the desired performance.

V. Conclusion

This paper analyzed the performance of UAV-aided RIS communication systems under practical impairments, namely UAV orientation deviations and RIS phase estimation errors, over Nakagami-m fading channels. Analytical expressions for the OP, ASER, and EC were derived using Gamma approximation and validated via Monte-Carlo simulations. The results demonstrate that both impairments significantly degrade system performance, with their combined effect causing more severe deterioration due to phase misalignment and beam misdirection. Moreover, key system parameters such as the number of RIS elements, fading severity, and phase error concentration were shown to strongly influence system reliability and capacity. Overall, the findings highlight the importance of incorporating practical impairments in the design of UAV-mounted RIS systems to ensure reliable and efficient communication in real-world scenarios.

Acknowledgment

This research was supported by MeitY under the SwaYaan program (Ref. No. POC-Y3-01-IIT-ID-01) and the 5G Use Case Lab at IIT Indore, funded by the DoT, Govt. of India.

References

[1] Q. Wu and R. Zhang,"Towards smart and reconfigurable environment: Intelligent reflecting surface aided wireless network," *IEEE Commun. Mag.*, vol. 58, no. 1, pp. 106–112, Jan. 2020.

[2] Y. Zeng, Q. Wu, and R. Zhang,"Accessing from the sky: A tutorial on UAV communications for 5G and beyond," *Proc. IEEE*, vol. 107, no. 12, pp. 2327–2375, 2019.

[3] X. Pang *et al.*, "When UAV meets IRS: Expanding air-ground networks via passive reflection," *IEEE Wirel. Commun.*, 2021, 28, 164–170.

[4] M. Aldababsa *et al.*, "Multiple RISs-aided networks: Performance analysis and optimization," *IEEE Trans. Veh. Technol.*, vol. 72, no. 6, pp. 7545–7559, Jun. 2023.

[5] V.-D. Phan *et al.*, "Performance of cooperative communication system with multiple reconfigurable intelligent surfaces over Nakagami-m fading channels," *IEEE Access*, vol. 10, pp. 9806–9816, 2022.

[6] T. Shafique, H. Tabassum, and E. Hossain, "Optimization of wireless relaying with flexible UAV-borne reflecting surfaces," *IEEE Trans. Commun.*, vol. 69, no. 1, pp. 309–325, Jan. 2021.

[7] T. Wang *et al.*, "Outage probability analysis of RIS-assisted wireless networks with von Mises phase errors," *IEEE Wireless Commun. Lett.*, vol. 10, no. 12, pp. 2737–2741, Dec. 2021.

[8] M. J. Zakavi *et al.*, "UAV-mounted IRS (UMI) in the presence of hovering fluctuations: 3D pattern characterization and performance analysis," 2025. [Online]. Available: https://arxiv.org/abs/2504.16613

[9] A. Al-Hourani *et al.*, "Optimal LAP altitude for maximum coverage," *IEEE Wirel. Commun. Lett.*, vol. 3, no. 6, pp. 569–572, Dec. 2014.

[10] A. Al-Hourani and K. Gomez, "Modelling cellular-to-UAV path-loss for suburban environments," *IEEE Wirel. Commun. Lett.*, vol. 7, no. 1, pp. 82–85, 2018.

[11] P. Sharma, S. R., and A. T. Pham, "Comprehensive performance analysis of UAV-assisted mixed FSO-RF communication system with nonlinear energy harvesting," *IEEE Trans. Veh. Technol.,* pp. 1–16, 2026.